Research Article Vol. 64, No. 16 / 1 June 2025 / Applied Optics D69

applied optics

Nonseeded linewise temperature measurements by resonantly ionized photoemission thermometry in a Mach 4 Ludwieg tube

Walker McCord,[1] Aleksander Clark,[1] Zhili Zhang,[1,*] Shelby Ledbetter,[2] and Mark Gragston[2]

[1]The University of Tennessee-Knoxville, Knoxville, Tennessee 37996, USA
[2]The University of Tennessee Space Institute, Knoxville, Tennessee 37388, USA
*zzhang24@utk.edu

Received 17 February 2025; revised 7 March 2025; accepted 7 March 2025; posted 12 March 2025; published 3 April 2025

A one-dimensional (1D) thermometry using oxygen-tagging resonantly ionized photoelectron thermometry (O_2 RIPT) was employed to investigate thermal gradients within a Mach 4 Ludwieg tube. The Ludwieg tube is pulsed with a test duration of approximately 100 ms, providing a cold supersonic flow at Mach 4 ideal for studying aerothermal effects. This study focused on measuring freestream temperatures, capturing shock-induced heating behind a detached bow shock from a blunt cylinder, and resolving sharp temperature variations across a bow shock generated by a cylinder. The O_2 RIPT technique produced strong emission signals extending approximately 4 cm long, demonstrating its capability for precise temperature measurements in high-speed wind tunnel environments. The results confirm that O_2 RIPT is well-suited for applications in large-scale aerodynamic testing facilities, particularly in regions with strong compression effects, enabling the resolution of sharp thermal gradients. This method presents a promising solution for thermometry in dynamic flow conditions relevant to various experimental ground-test facilities.

https://doi.org/10.1364/AO.559582

1. INTRODUCTION

One of the primary challenges in hypersonic vehicle design is to mitigate aerodynamic heating, which could impose significant thermal loads, leading to catastrophic structure failures during the flight. At high supersonic and hypersonic velocities, vehicles generally adopt a blunt-nosed configuration to manage heat transfer effectively and facilitate internal heat dissipation. The extent of bluntness, combined with the vehicle's speed, dictates the formation of a detached bow shock or a normal shock ahead of the body. This shockwave serves as an energy conversion mechanism, transforming kinetic energy into thermal and chemical energy [1]. The resulting high-temperature region directly behind the shock leads to significant stagnation heating. However, the detached shockwave helps reduce heat flux to the vehicle's surface by redistributing energy into the surrounding airflow through compression effects, with additional heating occurring within the boundary layer [2]. Despite this thermal management benefit, detached shocks introduce an aerodynamic penalty, increasing the surface pressure and drag due to entropy changes. Various strategies, such as aerospikes, forward mass injection, and freestream energy deposition, have been explored to mitigate these drawbacks while preserving thermal protection [3–7].

The extreme temperatures and chemical reactions occurring in the post-shock region can lead to molecular dissociation, creating a complex non-equilibrium flow that poses challenges for computational fluid dynamics (CFD) modeling [8]. As a result, accurate experimental data are essential for validating numerical simulations. Given the need for reliable measurements in high-speed flow environments, non-intrusive optical diagnostics are preferred over intrusive probes, which can introduce disturbances and alter flow behavior. Optical thermometry techniques capable of capturing fine-scale thermal gradients are particularly valuable for these studies [9,10]. Several established methods, including planar laser-induced fluorescence (PLIF) [11], tunable-diode laser absorption spectroscopy (TDLAS) [12], filtered Rayleigh scattering [13], and coherent anti-Stokes Raman scattering (CARS) [10–14], have been employed to study aerodynamic heating around blunt bodies [15–17]. However, each technique has limitations: PLIF requires the addition of tracer molecules that may affect flow chemistry, TDLAS provides path-integrated data with limited spatial resolution [18–20], and filtered Rayleigh scattering relies on density-dependent signal intensity, making it less effective at low pressures. Since Rayleigh scattering is a linear optical process proportional to density, the overall signal intensity is low

at low-pressure conditions for temperature measurements in the supersonic tunnels. Seedings of CO_2 or water can increase the signal intensity, but the temperature is based on ideal gas law interpretation. CARS does not require flow seeding and is non-path integrated historically, making it an attractive option for single-point measurements in the wind tunnels. However, CARS requires relatively complex optical alignment paths to direct various beams to perfectly overlap spatiotemporally [10,14]. Furthermore, a high-fidelity, typically large spectrometer is required to analyze the signal with sufficient spatial resolution to obtain an accurate spectrum reading.

Oxygen-based resonantly ionized photoemission thermometry (O_2 RIPT) is an emerging diagnostic technique capable of measuring gas vibrational temperature along a one-dimensional (1D) profile in low-enthalpy, high-speed flows, all without requiring particle or gas seeding [15,16]. This method leverages developments in resonant enhanced multi-photon ionization (REMPI) to selectively excite oxygen molecules, leading to electron impact ionization of ambient nitrogen and the subsequent formation of N_2^+ ions [17–19]. The thermometric capability of O_2 RIPT is based on the well-established correlation [20–22] between the emission intensity of the first negative band of nitrogen, specifically N_2^+ ($B^2\sum_u^+ \rightarrow X^2\sum_{-g^+}$), and the two-photon transition probability within oxygen's absorption band, O_2 [$X^3\sum(v'')=0 \rightarrow C^3\Pi(v=2)$], spanning the 285–289 nm range. Because this emission process reflects the rotational state distribution of molecular oxygen, analyzing multiple resonant absorption transitions allows the construction of a Boltzmann-weighted distribution, which facilitates accurate temperature determination. Furthermore, since the observed emissions originate from nitrogen excitation due to oxygen ionization, the inferred temperature corresponds to the ro-vibrational states of the gas. The underlying REMPI physics governing O_2 RIPT signal generation has been extensively detailed in previous studies [23–25] and will not be reiterated here. For a more in-depth discussion on calibration and the assessment of O_2 RIPT's ability to determine gas temperatures, readers are encouraged to refer to an earlier validation study [21].

In this study, O_2 RIPT is employed to perform one-dimensional (1D) temperature measurements in a large-scale Mach 4 Ludwieg tube, marking its first implementation for gas-phase thermometry in a high-speed wind tunnel environment. The technique is initially applied to determine the freestream static temperature under steady-state conditions, with results compared against isentropic flow predictions. Subsequently, O_2 RIPT is utilized to capture the thermal gradient across a bow shock generated by a cylindrical model. This experiment highlights the effectiveness of 1D temperature diagnostics in resolving spatial temperature distributions within shock-dominated flow fields.

2. EXPERIMENT SETUP

A. Facility

The O_2 RIPT experiments were conducted in the UTSI Mach 4 Ludwieg tube, housed within the Tennessee Aerothermodynamics Laboratory (TALon). A CAD rendering of the tunnel is provided in Fig. 1 [21,25]. The wind tunnel features a nozzle exit measuring 61 cm × 61 cm (24 in × 24 in) and a 1.82 m (6 ft) long test section. Due to vacuum tank limitations and the high mass flow rate characteristic of the facility, the total operational duration is approximately 200 ms, with about 130 ms dedicated to steady-state flow conditions. For these experiments, the nominal total pressure and temperature were set at 439.7 kPa and 295 K, respectively. The corresponding static conditions were approximately 2.89 kPa for pressure and 70.2 K for temperature. The freestream Reynolds number per meter was determined to be 21.2×10^6 m^{-1}, providing a representative flow environment for high-speed aerothermal studies.

B. Optical Setup

The laser system employed for O_2 RIPT measurements consisted of an injection-seeded Nd:YAG laser (Spectra Physics Quanta Ray Pro 290), operating at a second harmonic wavelength. This laser, with a pulse width of 8 ns, a repetition rate of 10 Hz, and an average pulse energy of 1 J, was used to pump a dye laser (Sirah PrecisionScan). The dye laser, utilizing a blend of Rhodamine 590 and Rhodamine 610, produced lasing light near 574 nm with a linewidth of approximately 0.02 cm^{-1}. Frequency doubling of this output generated deep ultraviolet (UV) radiation centered around 287 nm, effectively targeting the O_2 [$[X^3\sum(v'=0) \rightarrow C^3\Pi(v=2)]$] resonant absorption band. The system consistently delivered nominal pulse energies of approximately 30 mJ per pulse across the 285–288 nm wavelength range.

To ensure precise beam delivery, the UV light was directed vertically using a UV fused silica right-angle prism before being focused with a fused silica plano-convex lens ($f = 500$ mm). This configuration was carefully chosen to allow the laser beam to pass unobstructed through the tunnel's fused silica windows while maintaining the high intensity required for multiphoton absorption at the test section's center. The resulting O_2 RIPT signal was captured using an intensified scientific camera (PI-MAX4 1024f) equipped with a 1000 mm focal length lens. The camera's 1024 × 1024 pixel sensor provided high-resolution imaging of the signal. To minimize interference from laser scattering and background illumination, a 50 mm × 50 mm Schott BG3 optical filter (1 mm thick) was positioned in the optical path. A complete view of the experimental setup within the TALon lab is shown in Fig. 2.

C. Tunnel Test Models

Besides freestream temperature measurements, O_2 RIPT was also applied to capture temperature distributions in the vicinity of a test model. First, a cylindrical model was used to generate a strong normal shock, creating an environment relevant for studying shock-wave compression heating effects. The interaction of viscous dissipation and turbulent flow mixing behind the detached shockwave resulted in a high-temperature region, making it an ideal case for evaluating O_2 RIPT's capability in measuring through shock temperature variations. Additionally, this experiment helped establish the technique's robustness in capturing steep thermal gradients in complex flow conditions. The test model consisted of a 25.4 mm diameter, 10.16 cm long

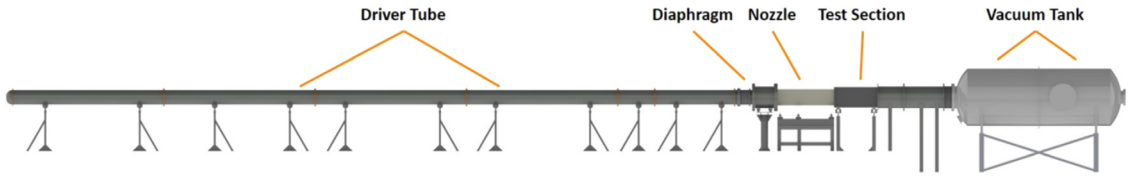

Fig. 1. A rendering of the UTSI Mach 4 Ludwieg tube.

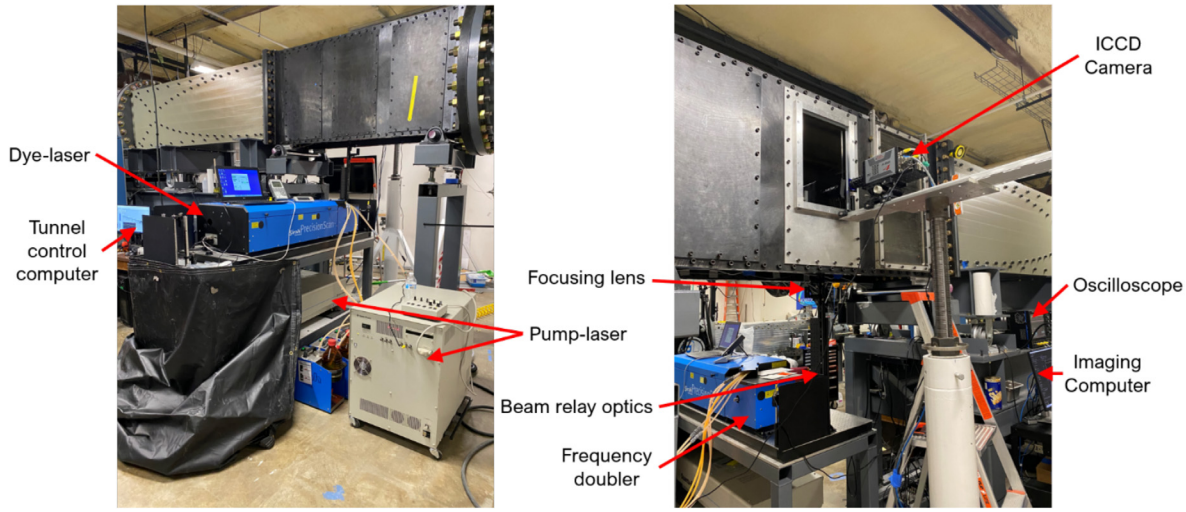

Fig. 2. O_2 RIPT setup for the Mach 4 tunnel. Key components were identified with arrows, including pump laser, dye laser, beam optics, and tunnel control computer on the left image, and ICCD camera, oscilloscope, and imaging capture computer on the right image.

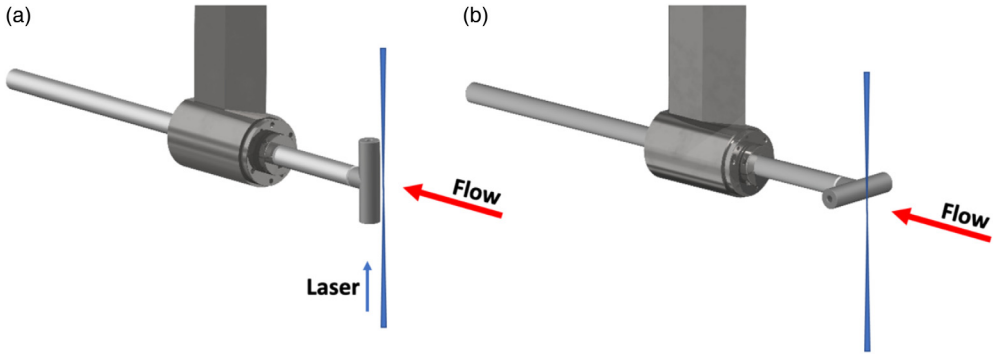

Fig. 3. (a) Cylindrical model in the vertical orientation and (b) the horizontal orientation. The focusing laser beam enters the tunnel from fused-silica windows on the floor of the tunnel. The hammer is 10 cm long with a diameter of 4 cm.

cylinder, fabricated using a Form 3L 3D printer. It was mounted on a 700 cm long translation rod, allowing precise positioning along the tunnel axis to ensure optimal laser alignment. The UV laser beam was focused 3 mm away from the model's surface—chosen as the closest feasible distance to prevent laser-induced breakdown while accounting for tunnel motion during test runs. To minimize unwanted reflections, black photography tape was applied to the model's surface. Second, two experimental configurations were employed. In the first setup, the cylinder was positioned vertically (perpendicular to the tunnel floor), enabling the O_2 RIPT measurement line to extend along the model's surface and behind the detached shock. In the second configuration, the cylinder was oriented horizontally (parallel to the tunnel floor), allowing the measurement line to pass through the shock from the freestream, capturing the thermal transition across it. Computer-generated renderings of the vertical and horizontal orientations are depicted in Figs. 3(a) and 3(b), respectively.

3. RESULTS AND DISCUSSION

The O_2 $C^3\Pi$, $(v = 2) \leftarrow X^3\Sigma(v' = 0)$ absorption band can be used to produce laser emission generated N_2^+ photoemissions from locally available nitrogen in the flows. These photoemissions are directly related to the rotational line strength in the O_2 absorption band and, thus, are representative of the Boltzmann distribution of oxygen in the ground state. Various rotational peaks were identified to allow a gas temperature to be statistically

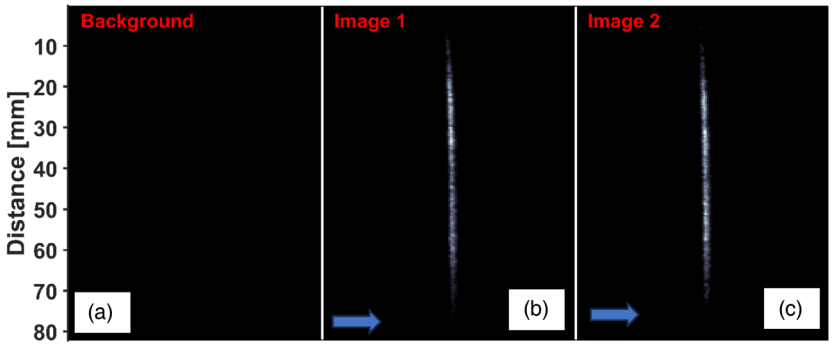

Fig. 4. Background image in (a) before the tunnel run showing no RIPT signal at low pressure, and raw images in (b) and (c) showing the O_2 RIPT emissions from 287.33 nm laser excitation in a Mach 4 freestream as collected from one run of the Mach 4 tunnel. The flow direction is indicated by the arrows in the figure.

determined. This enables the direct imaging capability along a line of generated emissions. The resulting photoemissions are related to temperature using Eq. (1), where E_{g_n} is the ground state energy of molecular oxygen, I_{λ_n} is the emission intensity at a laser excitation wavelength "n," T is the medium temperature, $T^2_{f_n,g_n}$ is two-photon absorption cross-section of molecular oxygen, and k_B is the Boltzmann constant [22]:

$$-\frac{1}{k_B T} \propto \log\left(\frac{I_{\lambda_n}}{T^2_{f_n,g_n}}\right)/E_{g_n}. \tag{1}$$

A. 1D Temperature Measurements in Mach 4 Freestream

O_2 RIPT measurements were performed to determine the freestream temperature within the test section, capturing data along a ~5 cm measurement line. Based on a prior calibration study [21], four specific probe wavelengths were selected using a reference temperature of 180 K. This temperature was chosen as it closely approximates the expected theoretical static freestream temperature of 72 K within the tunnel. To generate the O_2 RIPT measurement line, the laser was focused using a 300 mm plano-convex lens, ensuring optimal positioning within the test section while minimizing interference from wall boundary layer scattering. Given the constraints of steady-state tunnel operation and laser repetition rates, only two single-shot RIPT signals could be recorded per wavelength. A pre-run baseline image, along with the RIPT signal image at 287.33 nm excitation, is provided in Fig. 4(a).

Prior research on signal-pressure dependence in enclosed environments has demonstrated that as pressure decreases from atmospheric levels, emission strength diminishes significantly, becoming indistinguishable from background noise at approximately 41.4 kPa (6 Psia) [26]. Despite the low static freestream pressure of approximately 2.89 kPa (0.41 Psia) in the current Mach 4 conditions, strong photoemission signals were still successfully generated. The reduced temperature and pressure of the supersonic flow further mitigated quenching effects, enhancing signal lifetime. These combined factors resulted in photoemission intensities exceeding those recorded under standard temperature and pressure conditions.

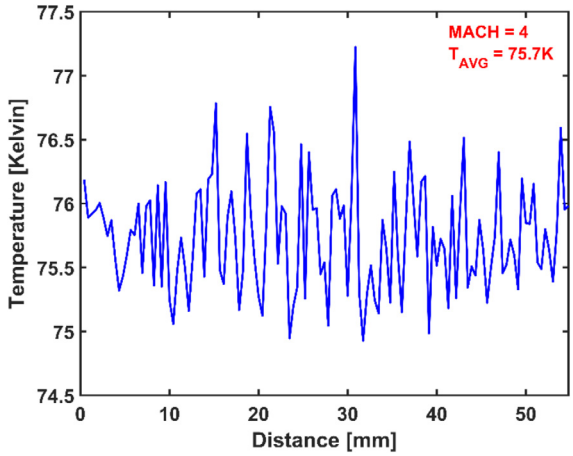

Fig. 5. O_2 RIPT line temperature measurement of the Mach 4 tunnel freestream, showing an average temperature of ~75.7 K with fluctuations of ±1 K. The theoretical isentropic flow temperature is ~72 K.

Under the current Mach 4 conditions, REMPI-generated electrons dominate the signal, and background ionization is not expected to contribute significantly. However, in hypersonic flows, shock-induced ionization may introduce additional free electrons, which could interfere with the measurement. In such cases, distinguishing REMPI-generated signals from background electrons may require time-resolved diagnostics or alternative spectroscopic techniques to ensure accurate temperature interpretation.

The images were post-processed using the same approach and equations discussed in previous work [21,26] to relate the photoemission strength to the ro-vibrational temperature. Basically, the temperature was determined by using Eq. (1) for each pixel in the image. The resulting O_2 RIPT temperature measurement of the free stream across a 52 mm line length is shown in Fig. 5. The imaging camera used a 1000 mm telephoto focusing lens for imaging, which magnified the photoemission line to significant spatial clarity where the spatial resolution became hardware limited (i.e., 13 μm). The average measured free stream temperature by O_2 RIPT was approximately 75.7 K, with mean fluctuations of approximately ±1 K. Slight temperature drops at the pixel level from viscous mixing, dissipation

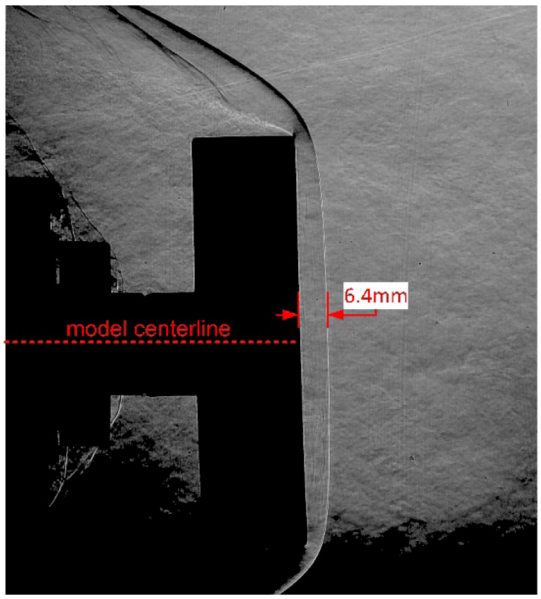

Fig. 6. A Schlieren image of the vertically oriented cylinder model in the Mach 4 flow. The shock standoff distance was determined to be 6.4 mm for these conditions. The slight angle of the model in the Schlieren imaging is due to a subtle 3D printing error but had no significant impact on the flow.

forces within the flow, camera readout noise, and shot-to-shot fluctuations in laser energy all contributed to the observed fluctuations. Isentropic flow theory is used to compare and validate the O_2 RIPT measurement. If considering non-heated, low-enthalpy Mach 4 conditions such as $T/T_0 = 0.238$, then the theoretical freestream static temperature is approximately 72 K. If the ±3 K associated error of the O_2 RIPT technique is considered, then the experimental values show relatively good agreement with the expected temperature values. Furthermore, if non-idealized flow parameters are considered, the O2 RIPT measurement may be a better representation of the actual flow temperature.

B. 1D Temperature Measurements with a Cylinder: Vertical Orientation

O_2 RIPT measurements were obtained by directing the laser beam along the center of a cylinder model oriented vertically and focusing the beam such that the beam waist was positioned centered vertically and horizontally on the model, as shown in Fig. 3(a). Furthermore, the beam was orthogonally offset from the model by 3 mm (i.e., upstream). It was necessary to offset the beam from the model as the tunnel is designed to move on rollers during runs to reduce the loads exerted on the supporting structures. To provide a better understanding of the flow field and estimate shock standoff distance, Schlieren imaging and computations were done prior to testing. Schlieren images were acquired at 50 kHz rates to examine the shock stability and characterize the stand-off distance. An instantaneous Schlieren image of the model in the Mach 4 flow is shown in Fig. 6. From the Schlieren image, it was found that the shock stand-off distance at the centerline of the model is approximately 6.4 mm from the model surface.

Computations of the flow field with the model were conducted using ANSYS Fluent to provide a quantitative comparison of the experimental data. The RANS simulations used the Spalart–Allmaras turbulence model and were done with varying mesh sizes to ensure sufficient convergence. The initialization parameters were based on the tunnel static conditions and velocity. The results for the Mach number and static temperature fields are shown in Figs. 7(a) and 7(b), respectively. The shock standoff distance according to the CFD was approximately 7.2 mm.

Figure 8(a) shows an experimentally collected raw image of the RIPT signal and the model location artificially added to the image to aid in line stand-off distance visualization. Using compressible flow theory and an assumed freestream temperature of 72 K results in a static temperature behind the shock of 295 K. The O_2 RIPT measurement predicted an average temperature of 296.5 K (±2% error) across a 1 in. line, which is depicted in Fig. 8(b). The average experimental value is well within the expected value, both showing great agreement with only slight deviations observed. Furthermore, since the difference between experimental and expected values is almost identical to that of the free stream measurement, this further indicates that the tunnel free stream temperature is slightly higher than the theoretical value.

C. 1D Temperature Measurement with a Cylinder: Horizontal Orientation

The generated O_2 RIPT measurement line used for thermometry measurements across the horizontal orientation of the model was approximately 4.0 cm in length, which was sufficient to cross the shock, measuring temperatures from both the free stream and behind the shock. The O_2 RIPT-generated line crossed the shock at approximately half the line length, allowing 2.0 cm line temperature assignments for both outside and behind the shock. A raw image of the RIPT signal for the horizontal orientation is shown in Fig. 9(a), with the approximate cylinder overlaid to aid in spatial placement with respect to the O_2 RIPT line. Due to the 3D relief effects, there exists a thermal gradient across the diameter of the model, with highest total temperatures located along the axis of the cylinder where stagnation effects are most prevalent.

The resulting emissions were post-processed in a similar fashion to the vertical study, except a code was used that monitored the coefficient of correlation for the individual pixel fits. This was done to allow the code to know when to switch from using the 180 K wavelengths to the 293 K wavelengths for temperature assignments [20]. This method was used as it yielded the highest accuracy and overall best gas temperature assignment, and the results are visualized in Fig. 9(b). The portion of the generated O_2 RIPT line that was within the free stream assigned an average gas temperature of approximately 75.2 K, aligning well with the theoretical and previous free stream measurement. The portion of the signal that was behind the shock demonstrated sufficient sensitivity to resolve the thermal gradient due to the 3D relief effects, with a max gas temperature assignment of 296 K at the model centerline.

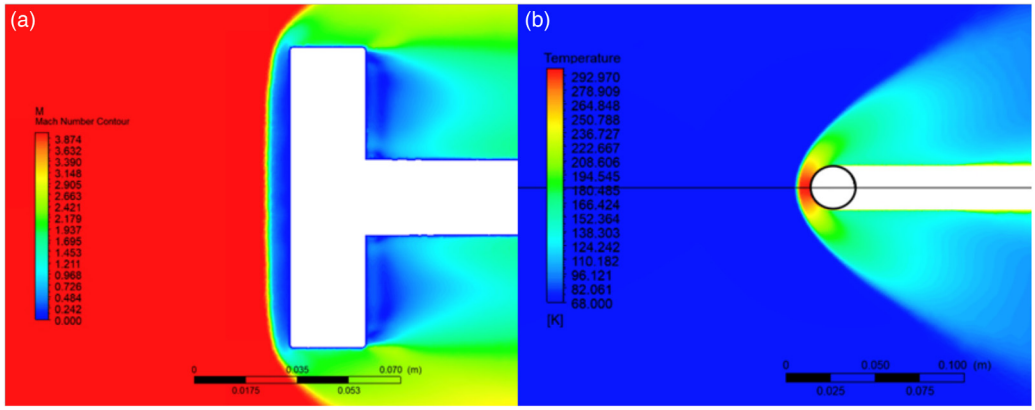

Fig. 7. Computational fluid dynamics calculation of the cylinder model in Mach 4 flows, showing (a) Mach contours and (b) the temperature contours along planes of symmetry.

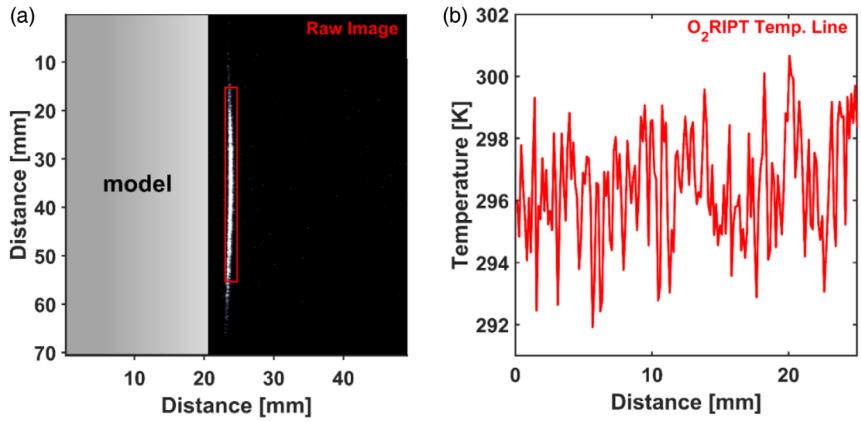

Fig. 8. (a) Single-shot image of model and O_2 RIPT line in Mach 4 flow and (b) O_2 RIPT temperature measurement behind shock.

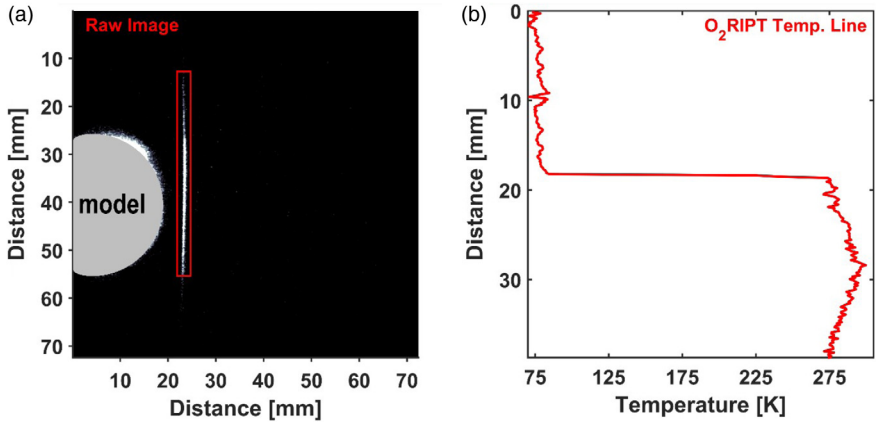

Fig. 9. (a) Overlaid image of the horizontal model and generated O_2 RIPT line and (b) O_2 RIPT temperature measurement across the shock. The sharp change in temperature values is due to the O_2 RIPT line passing through the shockwave.

4. SUMMARY AND CONCLUSION

This study has demonstrated the effectiveness of molecular oxygen-based resonantly ionized photoemission thermometry (O_2 RIPT) for one-dimensional temperature measurements spanning approximately 5.2 cm in a Mach 4 wind tunnel environment. Initially, the technique was used to measure the freestream temperature within the test section, capturing data along a 5.2 cm O_2 RIPT signal line. Given the non-heated, low-enthalpy nature of the tunnel, the expected theoretical static temperature was approximately 70.2 K—well outside the range of previous O_2 RIPT demonstrations [21,26,27]. The experimentally determined vibrational temperature averaged 75.7 ± 3 K, aligning closely with isentropic flow predictions within the measurement uncertainty. These results support the broader applicability of previously established O_2 RIPT calibration wavelengths for low-temperature gas environments (<293 K) [23].

To further assess O_2 RIPT's ability to capture temperature gradients, a cylindrical model was introduced to generate a strong detached shock. In the first configuration, the model was positioned vertically within the test section, allowing temperature measurements behind the shock along the cylinder's face. The 2.5 cm O_2 RIPT line yielded an average vibrational temperature of approximately 296 K. Normal shock relations predict a temperature increase by a factor of 4.07, which, when applied to the theoretical freestream temperature, results in an expected post-shock temperature of 295 K. The strong agreement between O_2 RIPT measurements and theoretical stagnation temperatures suggests the technique's reliability. The slight discrepancies observed may be attributed to the increased local gas density behind the shock, which enhances signal strength and improves the signal-to-noise ratio (SNR). In the second configuration, the cylinder was rotated by 90 deg, orienting its main axis parallel to the tunnel sidewalls. In this horizontal orientation, a 4.0 cm O_2 RIPT measurement line was used to capture both pre- and post-shock temperatures. The freestream portion of the measurement line recorded an average gas temperature of approximately 75.2 K, in agreement with theoretical and previously obtained values. Meanwhile, the post-shock region exhibited a well-resolved thermal gradient influenced by three-dimensional relief effects, with measured temperatures ranging from 276 K at the shock crossing to 296 K at the model's centerline.

Comparisons between the two orientations validated O_2 RIPT's ability to accurately capture temperature distributions in complex flow environments. Experimental results were benchmarked against theoretical models, computational fluid dynamics (CFD) simulations, and cross-shock measurements, all of which showed strong agreement. The CFD results further confirmed the measured thermal gradient behind the shock, with the predicted stagnation temperature at the model centerline closely matching the 296 K average obtained experimentally. The overlap between vertical and horizontal configuration measurements reinforces the accuracy of laser focusing and confirms spatial alignment between the two test conditions.

Future work will focus on expanding the application of O_2 RIPT to higher enthalpy conditions, improving spatial resolution, and integrating additional validation techniques to further refine temperature measurement accuracy in hypersonic environments. The continued development of this technique will enhance its utility for high-speed flow diagnostics and provide critical data for validating computational models of aerothermal phenomena.

Funding. National Science Foundation (2026242); University of Tennessee; U.S. Department of Energy.

Acknowledgment. The authors would like to acknowledge Kirk Davenport of the University of Tennessee Space Institute for support with the Mach 4 facility.

Disclosures. The authors declare no conflicts of interest.

Data availability. Data underlying the results presented in this paper are not publicly available at this time but may be obtained from the authors upon reasonable request.

REFERENCES

1. A. J. Eggers, H. J. Allen, and S. E. Neice, *A Comparative Analysis of the Performance of Long-range Hypervelocity Vehicles* (National Advisory Committee for Aeronautics, 1957), Vol. **1382**.
2. R. Mehta, "Numerical heat transfer study around a spiked blunt-nose body at Mach 6," Heat Mass Transfer **49**, 485–496 (2013).
3. C. D. Marley and D. W. Riggins, "Numerical study of novel drag reduction techniques for hypersonic blunt bodies," AIAA J. **49**, 1871–1882 (2011).
4. K. Zhong, C. Yan, S.-S. Chen, *et al.*, "Aerodisk effects on drag reduction for hypersonic blunt body with an ellipsoid nose," Aerosp. Sci. Technol. **86**, 599–612 (2019).
5. D. Riggins, H. F. Nelson, and E. Johnson, "Blunt-body wave drag reduction using focused energy deposition," AIAA J. **37**, 460–467 (1999).
6. S. R. Alexander, *Results of Tests of Determine the Effect of a Conical Windshield on the Drag of a Bluff Body at Supersonic Speeds* (National Aeronautics and Space Administration Hampton Va Langley Research Center, 1947).
7. M. B. Gerdroodbary, M. Imani, and D. Ganji, "Investigation of film cooling on nose cone by a forward facing array of micro-jets in hypersonic flow," Int. Commun. Heat Mass Transfer **64**, 42–49 (2015).
8. D. P. Schmidt, S. Gopalakrishnan, and H. Jasak, "Multi-dimensional simulation of thermal non-equilibrium channel flow," Int. J. Multiphase Flow **36**, 284–292 (2010).
9. P. Danehy, J. Weisberger, C. Johansen, *et al.*, "Non-intrusive measurement techniques for flow characterization of hypersonic wind tunnels," NF1676L-31725 (2018).
10. R. Miles, A. Dogariu, and L. Dogariu, "Localized time accurate sampling of nonequilibrium and unsteady hypersonic flows: methods and horizons," Exp. Fluids **62**, 248 (2021).
11. N. Jiang, M. Webster, W. R. Lempert, *et al.*, "MHz-rate nitric oxide planar laser-induced fluorescence imaging in a Mach 10 hypersonic wind tunnel," Appl. Opt. **50**, A20–A28 (2011).
12. S. E. Feltis, Z. Zhang, T. S. Dean, *et al.*, "Measurements of no rotational and vibrational temperatures behind a normal shock in hypervelocity flow via absorption spectroscopy," Exp. Fluids **65**, 112 (2024).
13. B. M. Richard, R. L. Walter, and N. F. Joseph, "Laser Rayleigh scattering," Meas. Sci. Technol. **12**, R33 (2001).
14. L. E. Dogariu, A. Dogariu, R. B. Miles, *et al.*, "Femtosecond laser electronic excitation tagging velocimetry in a large-scale hypersonic facility," AIAA J. **57**, 4725–4737 (2019).
15. W. McCord, A. M. Clark, Z. Zhang, *et al.*, "One-dimensional resonantly ionized photoelectron thermometry measurements in supersonic flow around a cylinder," in *AIAA SCITECH Forum* (American Institute of Aeronautics and Astronautics, 2023).
16. W. B. McCord, "Development and implementation of a novel resonantly ionized photoemission thermometry technique for one-dimensional measurements," in *Mechanical, Aerospace and Biomedical Engineering* (University of Tennessee Knoxville, 2022).
17. Z. Zhang, M. N. Shneider, and R. B. Miles, "Coherent microwave Rayleigh scattering from resonance-enhanced multiphoton ionization in argon," Phys. Rev. Lett. **98**, 265005 (2007).
18. J. Sawyer, Y. Wu, Z. Zhang, *et al.*, "O_2 rotational temperature measurements in an atmospheric air microdischarge by Radar REMPI," J. Appl. Phys. **113**, 233304 (2013).
19. S. F. Adams, J. C. A. DeJoseph, and J. M. Williamson, "Formation and electron-ion recombination of N4+ following photoionization in near-atmospheric pressure N2," J. Chem. Phys. **130**, 144316 (2009).
20. W. McCord, A. M. Clark, and Z. Zhang, "One-dimensional nitrogen-based resonantly ionized photoelectron thermometry (N_2 RIPT)," in *AIAA SCITECH Forum* (2023).
21. W. McCord, A. Clark, and Z. Zhang, "One dimensional air temperature measurements by air resonance enhanced multiphoton ionization thermometry (ART)," Opt. Express **30**, 18539–18551 (2022).
22. Z. Zhang, M. N. Shneider, and R. B. Miles, "Coherent microwave scattering from resonance enhanced multi-photon ionization (radar REMPI): a review," Plasma Sources Sci. Technol. **30**, 103001 (2021).

23. Y. Wu, J. Sawyer, Z. Zhang, *et al.*, "Flame temperature measurements by radar resonance-enhanced multiphoton ionization of molecular oxygen," Appl. Opt. **51**, 6864–6869 (2012).
24. Y. Wu, Z. Zhang, and S. F. Adams, "Temperature sensitivity of molecular oxygen resonant-enhanced multiphoton ionization spectra involving the C $^3\Pi_g$ intermediate state," Appl. Phys. B **122**, 149 (2016).
25. Y. Wu, Z. Zhang, and T. M. Ombrello, "Spatially resolved measurement of singlet delta oxygen by radar resonance-enhanced multiphoton ionization," Opt. Lett. **38**, 2286–2288 (2013).
26. W. McCord, M. Gragston, D. Plemmons, *et al.*, "O_2 based resonantly ionized photoemission thermometry analysis of supersonic flows," Opt. Express **30**, 40557–40568 (2022).
27. A. Dogariu, L. E. Dogariu, M. S. Smith, *et al.*, "Single shot temperature measurements using coherent anti-Stokes Raman scattering in Mach 14 flow at the Hypervelocity AEDC Tunnel 9," in *AIAA Scitech Forum* (2019).